Correlated heterogeneous dynamics in glass-forming polymers

H. Conrad,[1] F. Lehmkühler,[1,2,*] B. Fischer,[1,†] F. Westermeier,[1,‡] M. A. Schroer,[1,2] Y. Chushkin,[3] C. Gutt,[4] M. Sprung,[1] and G. Grübel[1,2]

[1]*Deutsches Elektronen-Synchrotron DESY, Notkestraße 85, 22607 Hamburg, Germany*

[2]*The Hamburg Centre for Ultrafast Imaging, Luruper Chaussee 149, 22761 Hamburg, Germany*

[3]*European Synchrotron Radiation Facility, Avenue des Martyrs 71, 38000 Grenoble, France*

[4]*University of Siegen, Walter-Flex Straße 3, 57072 Siegen, Germany*

(Received 14 January 2015; published 15 April 2015)

We report x-ray photon correlation spectroscopy experiments on the dynamics of the glass-former polypropylene glycol covering a temperature range from room temperature to the glass transition at $T_g = 205$ K using silica tracer particles. Three temperature regimes are identified: At high temperatures, Brownian motion of the tracer particles is observed. Near T_g, the dynamics is hyperdiffusive and ballistic. Around $1.12T_g$, we observe an intermediate regime. Here the stretching exponent of the Kohlrausch-Williams-Watts function becomes q dependent. By analyzing higher-order correlations in the scattering data, we find that dynamical heterogeneities dramatically increase in this intermediate-temperature regime. This leads to two effects: increasing heterogeneous dynamics and correlated motion at temperatures close to and below $1.12T_g$.

DOI: 10.1103/PhysRevE.91.042309 PACS number(s): 64.70.pj, 61.05.cf

I. INTRODUCTION

Although glasses are very common in everyday life, the transition from supercooled liquids to the glassy state is one of the mysteries in condensed matter physics (see [1–3] for a review). A majority of liquids comprising molecular liquids, colloidal liquids, and polymeric liquids form a glass if they are cooled or quenched fast enough to avoid crystallization. This is accompanied by a slowing down of the dynamics by several orders of magnitude around the glass transition temperature T_g. The structure of the sample, however, remains almost unchanged. In addition, upon approaching the glass transition, the observed relaxation phenomena become non-exponential, pointing to a broad distribution of the relaxation times and the existence of dynamical heterogeneities [3,4]. This is suggested to be closely connected to spatial heterogeneities where different local arrangements can be found within the liquid showing a variety of relaxation times [5]. Dynamical heterogeneities can be accessed by higher-order correlation functions as demonstrated in simulations [6–9]. Several experimental approaches have been developed to probe heterogeneous dynamics [3,10]. Among them are microscopy and dynamic light scattering techniques. They study mostly colloidal suspensions, foams, and colloidal gels [11–14] consisting of rather large particles. For dynamic light scattering the particles must be index matched with the suspending medium to avoid multiple scattering.

Such restrictions can be overcome by x-ray photon correlation spectroscopy (XPCS) [15]. By using x rays as a probe, the structure and dynamics can be studied on length scales ranging from colloidal systems [16,17] to atomic or molecular glasses [18–20]. Furthermore, the possibility of investigating heterogeneous dynamics via two-time correlations has been introduced recently [13,21]. In order to investigate the glass transition and gelation processes in soft matter systems, colloidal tracer particles have proven to be a powerful tool [22–27]. Probing the dynamics of neat solvents, e.g., polymers, is not possible with conventional XPCS for two reasons. The scattering signal at the position of the structure peak is too weak for XPCS. Moreover, the dynamics at such small (intermolecular) length scales is too fast to be measured by current array detectors. Introducing the tracer particles bypasses these two problems. The use of tracer particles allows one to access q values in the small-angle x-ray-scattering regime yielding decent scattering intensities and accessible time scales for XPCS in the range of milliseconds to several thousand seconds. At very low tracer particle concentrations with negligible particle-particle interactions, their dynamics is governed by the dynamics of the dispersion medium. In this way the dynamics of molecular systems can be investigated in the vicinity of the tracer particles using their strong x-ray-scattering signal. Caronna *et al.* [22] used silica tracer particles and reported a transition from Brownian motion at high temperatures to hyperdiffuse dynamics in supercooled propanediol. This transition was observed at $T \approx 1.2T_g$ and discussed in the context of cooperative dynamics at low temperatures. Similar observations were made by Guo *et al.* [23] and Hoshino *et al.* [24] studying tracer particles in different polystyrene samples. However, these studies could report only results down to temperatures of $1.1T_g$–$1.2T_g$ and dynamical heterogeneities were not addressed. The question arises as to how the dynamics changes at even lower temperatures in the vicinity of the glass transition. We want to extend this type of study to the glass transition temperature T_g using the model glass former polypropylene glycol. In addition, special attention is paid to the impact of dynamical heterogeneities to the various dynamical regimes encountered upon cooling.

*Corresponding author:felix.lehmkuehler@desy.de

†Current address: University of Hamburg, Grindelallee 117, 20146 Hamburg, Germany.

‡Current address: Max Planck Institute for the Structure and Dynamics of Matter, CFEL, Luruper Chaussee 149, 22761 Hamburg, Germany.

II. EXPERIMENT

A. Sample system

Polypropylene glycol (PPG) (Sigma Aldrich) with a molecular weight of 4000 g/mol consisting of approximately 68 propylene glycol monomers is a well known glass former. It has been studied covering bulk properties (see [28–30] and references therein) and surfaces [31–34]. It is difficult to crystallize [35,36] and its glass transition temperature is $T_g = 205$ K at a cooling rate of 2 K/min [37], which was used in this experiment.

Colloidal silica spheres were synthesized following a modified Stöber method [38] that allows the synthesis of almost monodisperse spherical particles with controlled particle sizes around 100 nm. Afterward, the particles were coated with [γ-(methacryloxy)propyl]trimethoxysilane, which lowers the effective charge of the silica particles and thus reduces the interparticle interaction [39]. After subsequent purification via dialysis in pure ethanol and filtering, the silica particles were transferred into PPG by mixing and evaporation of ethanol. Finally, particle volume fractions were adjusted to be below $\phi = 1\%$ to minimize particle-particle interactions of the silica spheres and to guarantee their tracer character.

B. Experimental procedure

The XPCS experiments were performed at beamlines ID10 of ESRF and P10 of PETRA III at DESY in small-angle x-ray-scattering (SAXS) geometry. At ID10, the photon energy was 8 keV with a beam size of 10×10 μm^2 defined by a compound refractive lens and roller blade slits. The samples were filled in quartz capillaries 1 mm in diameter with a wall thickness of 10 μm. The capillaries were vacuum sealed and placed in an evacuated cryo-SAXS sample chamber cooled by gaseous nitrogen flow and controlled by a temperature controller using impedance heaters [40]. The sample-detector distance was 5.2 m, using a MAXIPIX 2×2 detector (pixel size 55×55 μm^2) [41].

At P10 the photon energy was 7.9 keV with a beam size of 10×10 μm^2 defined by slits. The sample capillaries were placed into a cryo-SAXS chamber that was capable of covering a temperature range of 120–350 K [42]. The sample detector distance was set to 5 m using a Princeton Instruments (PI) LCX CCD detector with a pixel size of 20×20 μm^2.

In both experimental runs, additional SAXS patterns were taken from empty capillaries and capillaries filled with the pure glass former to determine their contributions to the scattering signal. First, the scattering patterns were analyzed to determine the size and size polydispersity of the silica particles. Afterward, the samples were measured at various temperatures between room temperature (295 K) and 205 K $= T_g$. The XPCS runs were started only after the temperature had stabilized (± 0.002 K) at the target point and after waiting for an additional waiting time to equilibrate ranging from 100 s at 295 K to more than 6000 s close to T_g. Series of several hundred diffraction patterns were taken at each temperature with typical exposure times of 0.1–0.3 s. At high temperatures even shorter exposure times were used. To prevent radiation damage the total beam exposure time was kept below 80 s. This threshold was determined for the samples in test exposures before the experiment. To cover slower relaxations, delay times between 0 and 12 s were added between the acquisition of two patterns depending on the temperature. During the delay the sample was not exposed to the radiation. In this way the experimental time window was increased to match the relaxation time at a particular temperature while the total exposure time was kept constant. In addition, a fresh sample spot was probed for each new temperature. In some cases, the x-ray beam was attenuated to balance the lifetime of the sample versus the optimum photon count rates.

Due to the slow readout of the PI camera, only dynamics with correlation times $\tau_c > 2$ s could be studied. These were observed for $T < 250$ K. The higher-temperature regime was therefore only accessible using the MAXIPIX detector, which offers frame rates up to 300 Hz. The diffraction patterns were corrected for background, flat field [43], and bad detector pixels afterward.

III. RESULTS

A. Sample characterization

In order to characterize the sample, SAXS patterns were analyzed in terms of particle size, size polydispersity, and volume fraction. Therefore, the form factor of a sphere using a Schultz-Flory size distribution was fitted to an azimuthally averaged intensity profile $I(q)$ of the dilute dispersion, yielding an average particle radius of $\bar{r} = 70.7$ nm and a size polydispersity of $\Delta r/\bar{r} = 5.2\%$. In this study, we will concentrate on dilute dispersions with negligible interparticle interactions. Thus, the silica particles only interact with the dispersion medium PPG and their dynamics are influenced directly by the dynamics of the glass-forming liquid. The static structure factor becomes $S(q) \approx 1$ and consequently $I(q)$ from the sample under study does not vary significantly from the measured particle form factor. Figure 1(a) shows such an azimuthally averaged intensity profile together with a fit of a form factor of polydisperse spheres $P(q)$ to the data. This result confirms that the particle-particle interactions are negligible and the volume fraction of the silica spheres is indeed below 1%.

B. XPCS results

The XPCS analysis was performed using the multispeckle technique [44]. The obtained intensity correlation functions g_2 are shown for a high temperature of $T = 295$ K [Fig. 1(b)] and a low temperature of $T = 222$ K [Fig. 1(c)] for selected q values. For simplicity, the functions are normalized to the speckle contrast β. Here β was found to be constant during each experiment, but may differ for different setups. As the exposure time at high temperatures had to be short to access time scales on the order of 0.01 s, only a limited q range was accessible. At larger q values the statistics was too poor to calculate g_2 functions. The g_2 functions were fitted with the Kohlrausch-Williams-Watts (KWW) function [45]

$$g_2(q,t) = \beta \exp\{-2[\Gamma(q)t]^{\gamma(q)}\} + 1. \quad (1)$$

The results are shown by the solid lines in Figs. 1(b) and 1(c). Here Γ denotes the relaxation rate, which is connected to the relaxation time via $\tau_c = \Gamma^{-1}$, and the stretching exponent γ,

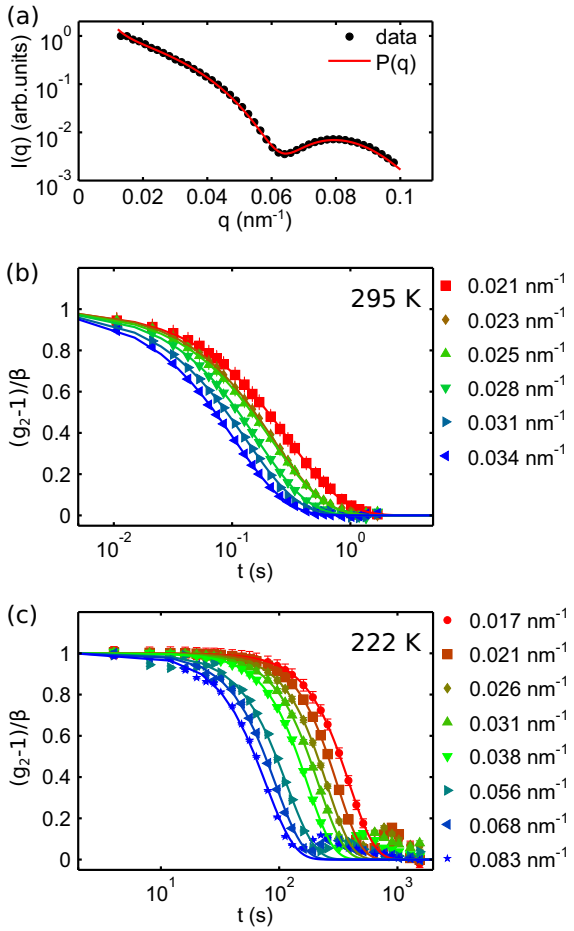

FIG. 1. (Color online) (a) Plot of $I(q)$ from the studied sample and particle form factor fit $P(q)$. (b) and (c) Intensity autocorrelation functions g_2 at different q values for (b) $T = 295$ K and (c) $T = 222$ K. Solid lines are fits with the KWW function (1). For 222 K additional contributions at longer time scales can be observed. In both cases the time axes cover three orders of magnitude.

which reflects the distribution of relaxation times about τ_c [46]. Obviously, the relaxation rate Γ decreases upon cooling, which reflects the slowing down of the particle dynamics. We found that the relaxation times follow a Vogel-Fulcher-Tammann behavior [3] for $T \geqslant 222\ \text{K} = 1.08T_g$, covering more than three orders of magnitude from 0.1 s (295 K) to several 100 s (222 K). This is accompanied by a change of slope of g_2 indicating a transition from normal ($\gamma \approx 1$) to compressed ($\gamma \approx 2$) exponential decay. This transition will be discussed in more detail below. At low temperatures [Fig. 1(c)], additional long time contributions can be observed on the order of 10% of the maximum contrast β. Below 222 K these contributions become more pronounced, while the first decay remains almost unchanged and the relaxation time fluctuates around few hundred seconds. The contributions are isotropic over the full q ring, which indicates the absence of any convective motion in the liquid, e.g., due to gravity. This would result in direction-dependent relaxation times accompanied by oscillations in the g_2 functions [47]. We will concentrate on the first decay.

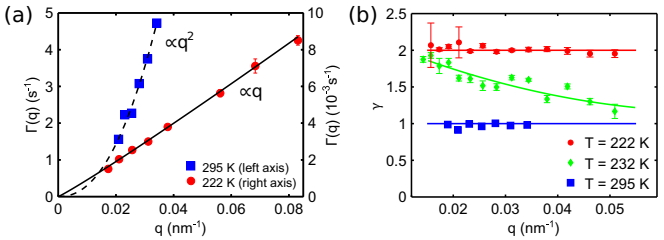

FIG. 2. (Color online) Dynamics at low and high temperature. (a) Relaxation rate $\Gamma(q)$. The left Γ axis corresponds to the results from 295 K (blue squares) and the right axis to the results from 222 K (red circles). Solid lines represent fits. (b) The q dependence of the stretching exponent γ for selected temperatures. Solid lines are guide to the eyes.

The results of the fits to the KWW function are shown in Fig. 2. First, we discuss the q dependence of the relaxation rate Γ at different temperatures. Therefore, we model $\Gamma(q)$ with a power law $\Gamma(q) = \Gamma_0 q^p$. As already observed from the g_2 functions, the relaxation rate Γ is found to grow with an exponent $p \approx 2$ (here $p = 2.2 \pm 0.2$ at $T = 295$ K). In contrast, with decreasing temperature this behavior changes to a linear increase with q ($p \approx 1$; here $p = 1.06 \pm 0.03$ at $T = 222$ K) [see Fig. 2(a)]. This suggests a transition from Brownian motion at high temperature ($p = 2$) towards ballistic motion after cooling ($p = 1$).

By taking a closer look to the shape of the g_2 function as expressed by the exponent γ, we observe an additional change from a simple exponential decay at 295 K ($\gamma \approx 1$) to a compressed one at 222 K with $\gamma > 1$. This is shown in Fig. 2(b), where γ is displayed as function of q for the corresponding temperatures. Most importantly, no distinct q dependence can be observed for 295 and 222 K. In contrast, a transition from $\gamma \approx 2$ at low q towards $\gamma \approx 1$ is obtained for intermediate temperatures around 232 K.

The overall behavior of p and γ is shown in Fig. 3. Three temperature regions can be defined: region A that is characterized by $p \approx 1$ and $\gamma \approx 2$ for $T \leqslant 222$ K, the intermediate region B around 230 K, and region C with $p \approx 2$ and $\gamma \approx 1$ for $T \geqslant 240$ K. As mentioned above, this suggests a transition from free diffusion at high temperatures (region C) to hyperdiffuse correlated dynamics upon cooling towards

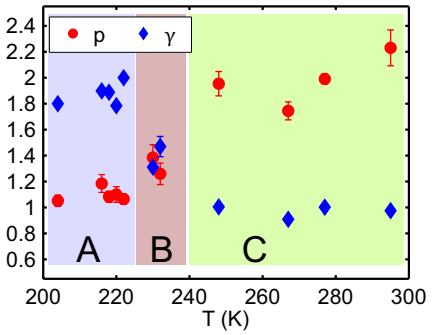

FIG. 3. (Color online) Temperature dependence of p and q-averaged γ. The temperature regions corresponding to different dynamical behavior are labeled by A, B, and C and different background colors.

T_g (region A). A more complex dynamics is observed in the transition region B around $T \approx 230$ K $\approx 1.12T_g$. Here γ becomes q dependent with an average of approximately 1.5. Similar results were obtained for slightly lower silica particle concentrations, also obeying the requirements for tracer particles. The change to hyperdiffuse dynamics is in line with recent studies on different glass formers [22–24] where such transitions were observed in a temperature region around $1.1T_g$–$1.2T_g$. However, due to experimental restrictions, these studies only reported the transition from C to B without accessing the low-temperature region A. The transition from C to B was successfully described by a continuous-time random-walk model [22,24]. Within this model, the q dependences of Γ and γ in particular in region B can be described more quantitatively, yielding the nature of the diffusivity and thus the dynamics of the sample. Another approach to obtain a deeper insight into the sample dynamics beyond g_2 functions is the study of two-time correlation functions. They allow one to quantify in particular the role and degree of dynamical heterogeneities in all three temperature regimes.

C. Two-time correlation functions and dynamic heterogeneities

In order to gain more insight into this dynamical crossover, we studied the instantaneous intensity correlation function [48]

$$C_I(q,t_1,t_2) = \frac{\langle I_p(q,t_1) I_p(q,t_2)\rangle_\psi}{\langle I_p(q,t_1)\rangle_\psi \langle I_p(q,t_2)\rangle_\psi}, \tag{2}$$

where $\langle\cdot\rangle_\psi$ denotes the average over pixels within the same momentum transfer $q \pm \Delta q$. Here the multispeckle time correlation scheme [49] is essential to overcome the time averaging in the g_2 function. The function C_I is typically used to study time-dependent out-of-equilibrium behavior, which is an important feature of glassy systems [50]. Here C_I measures the time evolution of the intensity autocorrelation function $g_2(q,\bar{t})$ along the absolute experimental time $t = (t_1 + t_2)/2$ for a delay time $\bar{t} = t_2 - t_1$. In the case of systems in equilibrium, the dynamics does not change with t and the time average of C_I is equal to g_2 via $g_2(q,t) = \langle C_\mathrm{I}(q,t_1,t)\rangle_{t_1}$. Two examples of C_I at $T = 222$ and 295 K at $q = 0.023$ nm^{-1} are shown in Figs. 4(a) and 4(b), respectively.

Temporal fluctuations as observable in Fig. 4(a) in equilibrium dynamics are assumed to play a key role in the dynamics of glass formers near T_g [3]. A useful quantity to describe the fluctuations of C_I is given by its normalized variance [13]

$$\chi_\mathrm{T}(q,t) = \frac{\left\langle C_\mathrm{I}^2(q,t_1,t)\right\rangle_{t_1} - \langle C_\mathrm{I}(q,t_1,t)\rangle_{t_1}^2}{\langle C_\mathrm{I}(q,t_1,t=0)\rangle_{t_1}^2}. \tag{3}$$

The normalized variance χ_T typically peaks around the inflection point of g_2. The height of the peak is proportional to the variance of the characteristic relaxation time ($\frac{\Delta\tau_c}{\tau_c}$), which is related to the width of the relaxation time distribution in the system. Thus, an increase of the peak height $\chi_{\mathrm{T}_\mathrm{max}}$ can be related to increasing dynamical heterogeneities in equilibrium systems.

Spatial heterogeneities, frequently expressed by the so-called four-point susceptibility χ_4 [51], which is a measure of the fraction of particles with correlated motion, is assumed to be the origin of the increasing dynamical heterogeneities near T_g [52]. While χ_4 is difficult to measure in experiments, χ_T has been studied in glassy materials to characterize dynamical correlation lengths [53] based on the assumption of a direct relation between χ_T and χ_4 [51]. The χ_T calculated for various q values from the data taken at 222 K is shown in Fig. 4(c). It should be noted that the evaluation of χ_T needs data of higher statistics than necessary, e.g., for the determination of g_2, resulting in fewer accessible q values. The dominating feature is the peaking of χ_T around the inflection point $t = \tau_c/e$ of g_2. The relatively high peak value on the order of 10^{-2} was also observed in colloidal gels and for surface dynamics of colloidal particles suspended in viscous liquids [53,54]. The height of the χ_T peak has a distinct q-related scaling proportional to q^p at small q [53] that is connected to the q dependence of $\tau_\mathrm{c}(T,q)$. In order to compare temporal fluctuations of dynamics at different temperatures q independently, it was proposed to use a normalized q-independent value ${\chi_\mathrm{T}}^* = \chi_\mathrm{T}\left(\frac{q}{q_0}\right)^p$ [53,55], where q_0 denotes a constant scaling factor. The averaged peak value $\xi(T) = \langle {\chi_\mathrm{T}}^*_\mathrm{max}\rangle_q$ over all q is shown in Fig. 4(d) for the sample discussed before (sample 1) and a similar sample at a slightly lower volume fraction (sample 2). Due to experimental constraints ξ could not be calculated for temperatures below 220 K. A pronounced increase of the peak height is clearly visible in region B while it stays almost constant at higher temperatures. This shows that the dynamics indeed becomes increasingly heterogeneous at temperatures around $T \approx 1.12T_g$. Taking into account the observations from the XPCS analysis, this may indicate the existence of rearranging cooperative regions as reported for many glass-forming systems [3]. An increasing peak value ξ has been identified as an identifying characteristic of growing length scales of such regions over which dynamics are cooperative [7,10,21,51]. This reveals that around $1.12T_g$ an increasing number of silica tracer particles exhibit cooperative dynamics that is fully governed by the growth of regions of cooperative dynamics in PPG of more than one order of magnitude in volume [54,56,57].

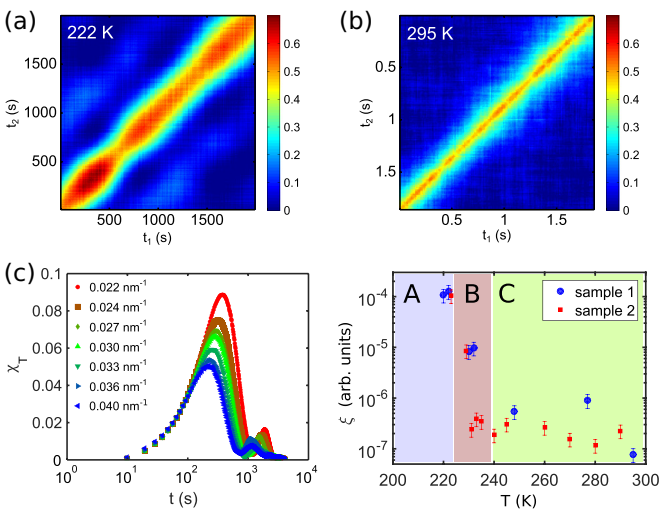

FIG. 4. (Color online) Two time correlation functions C_I for (a) 222 K and (b) 295 K at $q = 0.023$ nm^{-1}. (c) Plot of χ_T for 222 K. (d) Plot of $\xi(T)$ for two samples of slightly different volume fraction of tracer particles. The regions identified in Fig. 3 are indicated by A, B, and C and different background colors.

IV. CONCLUSION

We investigated the dynamical behavior of the glass former PPG with the help of tracer particles. The XPCS results indicated via the q dependence of the g_2 decay a change of the tracer particle dynamics with decreasing temperature. This is caused by the surrounding liquid. The dynamical crossover from diffusive to hyperdiffusive dynamics is found around $T \approx 1.12T_g$. In addition, the decay of g_2 becomes compressed in the hyperdiffusive regime, which is connected to an increasingly correlated particle motion. We interpret this crossover as a change of properties of the glass former. In contrast to previous studies [22–24], we were able to probe temperatures down to T_g (region A) showing hyperdiffuse correlated and heterogeneous dynamics. The increase of temporally heterogeneous dynamics was observed at the onset of hyperdiffusive dynamics. These findings suggest the growth of domains of correlated motion in the liquid close to T_g. While these are absent or too small at high temperatures (region C), where the tracer particles exhibit Brownian motion, their size is suggested to grow at intermediate temperatures. This is accompanied by the change to hyperdiffusive behavior. It has to be noted that additional long time contributions in g_2 at low temperatures (region A) are observed. This is in line with the heterogeneous nature of the sample dynamics at these temperatures. However, experimental limitations do not allow us to describe them quantitatively yet.

ACKNOWLEDGMENTS

We thank the Hamburg Centre for Ultrafast Imaging and the graduate school GRK1355 Physics with new advanced coherent light sources of the German Research Foundation for financial support. Parts of this research were carried out at the light source PETRA III at DESY, a member of the Helmholtz Association. We would like to thank O. Czakkel for assistance during the ESRF beamtime.

[1] C. Angell, Science **267**, 1924 (1995).
[2] P. Debenedetti and F. Stillinger, Nature (London) **410**, 259 (2001).
[3] L. Berthier and G. Biroli, Rev. Mod. Phys. **83**, 587 (2011).
[4] M. Ediger, Annu. Rev. Phys. Chem. **51**, 99 (2000).
[5] T. Kawasaki and H. Tanaka, J. Phys.: Condens. Matter **22**, 232102 (2010).
[6] W. Kob, C. Donati, S. J. Plimpton, P. H. Poole, and S. C. Glotzer, Phys. Rev. Lett. **79**, 2827 (1997).
[7] N. Lačević, F. Starr, T. Schrøder, and S. Glotzer, J. Chem. Phys. **119**, 7372 (2003).
[8] T. Kawasaki, T. Araki, and H. Tanaka, Phys. Rev. Lett. **99**, 215701 (2007).
[9] H. Tanaka, T. Kawasaki, H. Shintani, and K. Watanabe, Nat. Mater. **9**, 324 (2010).
[10] L. Berthier, G. Biroli, J.-P. Bouchaud, L. Cipelletti, and W. van Saarloos, *Dynamical Heterogeneities in Glasses, Colloids, and Granular Media* (Oxford University Press, New York, 2011).
[11] W. Kegel and A. van Blaaderen, Science **287**, 290 (2000).
[12] P. Mayer, H. Bissig, L. Berthier, L. Cipelletti, J. P. Garrahan, P. Sollich, and V. Trappe, Phys. Rev. Lett. **93**, 115701 (2004).
[13] A. Duri and L. Cipelletti, Europhys. Lett. **76**, 972 (2006).
[14] E. Weeks, J. Crocker, and D. Weitz, J. Phys.: Condens. Matter **19**, 205131 (2007).
[15] G. Grübel and F. Zontone, J. Alloys Compd. **362**, 3 (2004).
[16] F. Westermeier, B. Fischer, W. Roseker, G. Grübel, G. Nägele, and M. Heinen, J. Chem. Phys. **137**, 114504 (2012).
[17] P. Kwasniewski, A. Fluerasu, and A. Madsen, Soft Matter **10**, 8698 (2014).
[18] M. Leitner, B. Sepiol, L.-M. Stadler, B. Pfau, and G. Vogl, Nat. Mater. **8**, 717 (2009).
[19] B. Ruta, Y. Chushkin, G. Monaco, L. Cipelletti, E. Pineda, P. Bruna, V. M. Giordano, and M. Gonzalez-Silveira, Phys. Rev. Lett. **109**, 165701 (2012).
[20] B. Ruta, G. Baldi, Y. Chushkin, B. Rufflé, L. Cristofolini, A. Fontana, M. Zanatta, and F. Nazzani, Nat. Commun. **5**, 3939 (2014).
[21] A. Madsen, R. L. Leheny, H. Guo, M. Sprung, and O. Czakkel, New J. Phys. **12**, 55001 (2010).
[22] C. Caronna, Y. Chushkin, A. Madsen, and A. Cupane, Phys. Rev. Lett. **100**, 055702 (2008).
[23] H. Guo, G. Bourret, M. K. Corbierre, S. Rucareanu, R. B. Lennox, K. Laaziri, L. Piche, M. Sutton, J. L. Harden, and R. L. Leheny, Phys. Rev. Lett. **102**, 075702 (2009).
[24] T. Hoshino, D. Murakami, Y. Tanaka, M. Takata, H. Jinnai, and A. Takahara, Phys. Rev. E **88**, 032602 (2013).
[25] Y. Shinohara, H. Kishimoto, N. Yagi, and Y. Amemiya, Macromolecules **43**, 9480 (2010).
[26] B. Ruta, O. Czakkel, Y. Chushkin, F. Pignon, R. Nervo, F. Zontone, and M. Rinaudo, Soft Matter **10**, 4547 (2014).
[27] C. Passow, B. Fischer, M. Sprung, M. Köckerling, and J. Wagner, Langmuir **30**, 7283 (2014).
[28] C. León, K. Ngai, and C. Roland, J. Chem. Phys. **1110**, 11585 (1999).
[29] S. Rzoska and V. Mazur, *Soft Matter under Exogenic Impacts* (Springer, Dordrecht, 2007).
[30] K. Kaminski, W. Kipnusu, K. Adrjanowicz, E. Mapesa, C. Iacob, M. Jasiurkowska, P. Wlodarczyk, K. Grzybowska, M. Paluch, and F. Kremer, Macromolecules **46**, 1973 (2013).
[31] M. Sprung, T. Seydel, C. Gutt, R. Weber, E. DiMasi, A. Madsen, and M. Tolan, Phys. Rev. E **70**, 051809 (2004).
[32] Y. Chushkin, C. Caronna, and A. Madsen, Europhys. Lett. **83**, 36001 (2008).
[33] S. Streit-Nierobisch, C. Gutt, M. Paulus, and M. Tolan, Phys. Rev. B **77**, 041410(R) (2008).
[34] F. Lehmkühler, M. Paulus, S. Streit-Nierobisch, and M. Tolan, Fluid Phase Equilib. **268**, 95 (2008).
[35] S. Hager and T. Macrury, J. Appl. Polym. Sci. **25**, 1559 (1980).
[36] C. Angell and D. Smith, J. Phys. Chem. **86**, 3845 (1982).
[37] I. Park, K. Saruta, and S. Kojima, J. Therm. Anal. Calorim. **57**, 687 (1999).
[38] B. Fischer, T. Autenrith, and J. Wagner, Langmuir **26**, 6201 (2010).
[39] B. Maranzano, N. Wagner, G. Fritz, and O. Glatter, Langmuir **16**, 10556 (2010).

[40] R. Steinmann, Y. Chushkin, C. Caronna, J. Chavanne, and A. Madsen, Rev. Sci. Instrum. **82**, 25109 (2011).
[41] C. Ponchut, J. Rigal, J. Clément, E. Paillon, A. Homs, and S. Petitdemange, J. Instrum. **6**, C01069 (2011).
[42] H. Conrad, Ph.D. thesis, Hamburg University, 2014.
[43] A. Schavkan, F. Westermeier, A. Zozulya, S. Bondarenko, G. Grübel, C. Schroer, and M. Sprung, J. Phys. Conf. Ser. **425**, 202004 (2013).
[44] D. Lumma, L. Lurio, S. Mochrie, and M. Sutton, Rev. Sci. Instrum. **71**, 3274 (2000).
[45] G. Williams and D. Watts, Trans. Faraday Soc. **66**, 80 (1970).
[46] E. Hansen, X. Gong, and Q. Chen, Macromol. Chem. Phys. **214**, 844 (2013).
[47] S. Busch, T. Jensen, Y. Chushkin, and A. Fluerasu, Eur. Phys. J. E **26**, 55 (2008).
[48] A. Malik, A. R. Sandy, L. B. Lurio, G. B. Stephenson, S. G. J. Mochrie, I. McNulty, and M. Sutton, Phys. Rev. Lett. **81**, 5832 (1998).
[49] L. Cipelletti and D. Weitz, Rev. Sci. Instrum. **70**, 3214 (1999).
[50] L. Struik, *Physical Aging in Amorphous Polymers and Other Materials* (Elsevier, Amsterdam, 1978).
[51] L. Berthier, G. Biroli, J.-P. Bouchard, L. Cipelletti, D. E. Masri, D. L'Hote, F. Ladieu, and M. Pierno, Science **310**, 1797 (2005).
[52] R. Richert, J. Phys.: Condens. Matter **14**, R703 (2002).
[53] V. Trappe, E. Pitard, L. Ramos, A. Robert, H. Bissig, and L. Cipelletti, Phys. Rev. E **76**, 051404 (2007).
[54] A. Duri, T. Autenrieth, L.-M. Stadler, O. Leupold, Y. Chushkin, G. Grübel, and C. Gutt, Phys. Rev. Lett. **102**, 145701 (2009).
[55] E. Wandersman, E. Dubois, V. Dupuis, A. Duri, A. Robert, and R. Perzynski, J. Phys.: Condens. Matter **20**, 204124 (2008).
[56] O. Dauchot, G. Marty, and G. Biroli, Phys. Rev. Lett. **95**, 265701 (2005).
[57] A. Keys, A. Abate, S. Glotzer, and D. Durian, Nat. Phys. **3**, 260 (2007).